Disturbance Reduction Control Design for the ST7 Flight Validation Experiment

P. G. Maghami, O. C. Hsu, F. L. Markley, M. B. Houghton
NASA Goddard Space Flight Center
Guidance, Navigation and Control Division
Greenbelt, MD 20771

ABSTRACT

The Space Technology 7 experiment will perform an on-orbit system-level validation of two specific Disturbance Reduction System technologies: a gravitational reference sensor employing a free-floating test mass, and a set of micro-Newton colloidal thrusters. The ST7 Disturbance Reduction System is designed to maintain the spacecraft's position with respect to a free-floating test mass to less than 10 nm/$\sqrt{\text{Hz}}$, over the frequency range of 1 to 30 mHz. This paper presents the design and analysis of the coupled, drag-free and attitude control systems that close the loop between the gravitational reference sensor and the micro-Newton thrusters, while incorporating star tracker data at low frequencies. A full 18 degree-of-freedom model, which incorporates rigid-body models of the spacecraft and two test masses, is used to evaluate the effects of actuation and measurement noise and disturbances on the performance of the drag-free system.

INTRODUCTION

The Space Technology 7 (ST7) mission is a Disturbance Reduction System (DRS) flight validation experiment within NASA's New Millennium Program (NMP) [1]. New Millennium Program missions are intended to validate advanced technologies that have not flown in space in order to reduce the risk of their infusion into future NASA Space Science missions. The ST7 DRS incorporates two specific technologies: a highly sensitive Gravitational Reference Sensor (GRS), to measure the position and attitude of a spacecraft with respect to an internal free-floating test mass, and a set of micro-Newton colloidal thrusters to provide low-noise control of the spacecraft for drag-free flight. The ST7 DRS, scheduled to fly on the European Space Agency's SMART-II spacecraft in 2006, is designed to maintain the spacecraft's position, with respect to the GRS free-floating test mass, to less than 10 nm/$\sqrt{\text{Hz}}$, over ST7's science measurement frequency range from 1 to 30 mHz. This requirement will help ensure that the residual accelerations on the test masses (beyond gravitational acceleration) will be below the ST7 goal of $3\text{x}10^{-14}$ $(1 + [\text{f}/3\text{ mHz}]^2)$ m/s^2/$\sqrt{\text{Hz}}$. The SMART-II spacecraft will operate in an Earth-Sun L_1 drift-away orbit. The DRS instrument package consists of two gravitational reference sensors, two sets of four micro-Newton thrusters each for position and attitude control, an interferometer to measure the distance between the two test masses, and associated electronics.

This paper presents the overall design and analysis of the spacecraft drag-free and attitude controllers being designed by NASA's Goddard Space Flight Center. These controllers close the loop between the GRS and the micro-Newton colloidal thrusters. An 18-DOF model has been developed to capture the essential dynamics of the ST7-DRS package. It includes all rigid-body dynamics of the spacecraft and two test masses (three translations and three rotations for the spacecraft and each of the test masses). Actuation and measurement noise and major disturbance sources acting on the spacecraft and test masses are modeled. The ST7 DRS comprises three control systems: the attitude control system (ACS) to maintain a sun-pointing attitude, the drag free control (DFC) to center the spacecraft about the test masses, and the test mass suspension control. This paper extends the previous work on a two-dimensional 7-DOF Model of the ST7-DRS [2-3]. It summarizes the design and analysis for each of these systems, with particular attention given to the attitude and drag-free control systems.

MODEL DESCRIPTION

A schematic representation of the 18-DOF Model is shown in Figure 1. The location and the orientation of the two test masses can be arbitrarily assigned. The nominal position vectors for the two test masses and their respective housings are chosen as $p_1 = [-0.1 \quad 0.05 \quad 0.3]^T m$ and $p_2 = [0.1 \quad 0.05 \quad 0.3]^T m$, which means that the sensitive axis is along the X-axis of the spacecraft. Two clusters, each containing four thrusters, are located on the ±X faces to provide thrust capability for attitude and drag-free control. The centers of the thruster clusters are placed at $c_1 = [-0.9 \quad 0 \quad 0.25]^T m$ and $c_2 = [0.9 \quad 0 \quad 0.25]^T m$, respectively. Each thruster can provide a force that is variable from 2 μN to 20 μN in 0.1 μN increments. The clusters are mounted on the spacecraft as shown in Figure 2. Note that the distance between the lines of force of the pairs 1-3, 2-4, 5-7, and 6-8, which produce torque about the *x*-axis, is only 0.1 m, hence the resulting torque authority about the x-axis is limited. The force **F** and torque **T** on the spacecraft are related to the individual thrusts arrayed in a eight-dimensional vector **τ**, by:

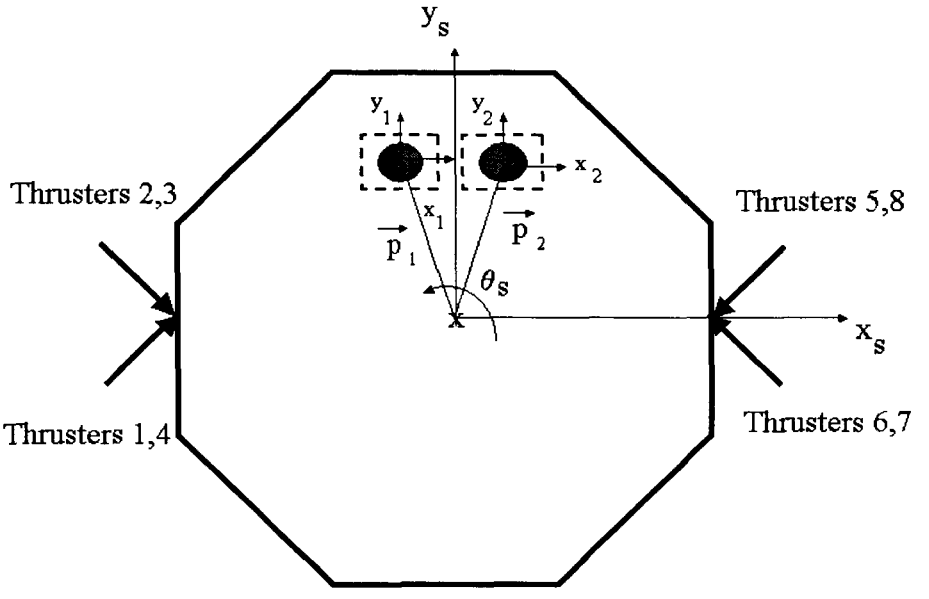

Figure 1 Schematic of the 18-DOF Model

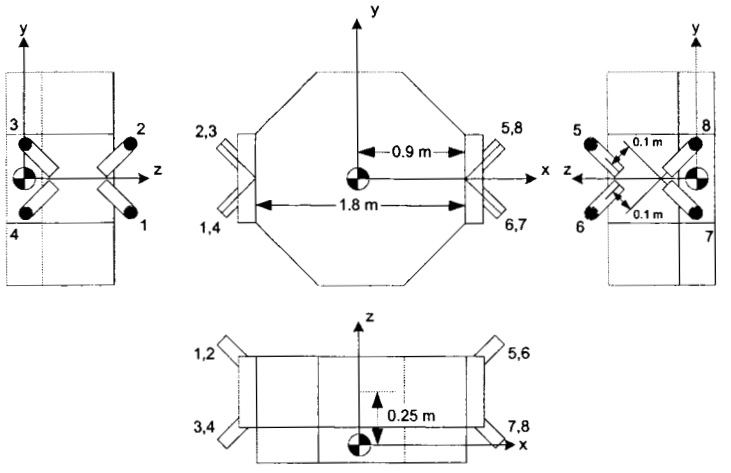

Figure 2 ST7 DRS Configuration on SMART-II

$$\begin{bmatrix}\mathbf{F}\\ \mathbf{T}\end{bmatrix} = H_{auth}\tau = \begin{bmatrix} 0.7071 & 0.7071 & 0.7071 & 0.7071 & -0.7071 & -0.7071 & -0.7071 & -0.7071 \\ 0.5000 & -0.5000 & -0.5000 & 0.5000 & -0.5000 & 0.5000 & 0.5000 & -0.5000 \\ -0.5000 & -0.5000 & 0.5000 & 0.5000 & -0.5000 & -0.5000 & 0.5000 & 0.5000 \\ -0.1604 & 0.1604 & 0.0896 & -0.0896 & 0.1604 & -0.1604 & -0.0896 & 0.0896 \\ -0.2232 & -0.2232 & 0.5678 & 0.5678 & 0.2232 & 0.2232 & -0.5678 & -0.5678 \\ -0.4500 & 0.4500 & 0.4500 & -0.4500 & -0.4500 & 0.4500 & 0.4500 & -0.4500 \end{bmatrix}\tau \quad (1)$$

The control authority matrix H_{auth} has rank six, as is required to control six degrees of freedom. In order to generate a desired force and thrust, the individual thruster commands are computed using the pseudoinverse of the authority matrix:

$$\tau_{cmnd} = H_{dist}\begin{bmatrix}\mathbf{F}_{desired}\\ \mathbf{T}_{desired}\end{bmatrix} = \begin{bmatrix} 0.2549 & -0.6339 & -0.25 & -3.5355 & -0.3125 & -0.2778 \\ 0.2549 & 0.6339 & -0.25 & 3.5355 & -0.3125 & 0.2778 \\ 0.0987 & -1.1339 & 0.25 & -3.5355 & 0.3125 & 0.2778 \\ 0.0987 & 1.1339 & 0.25 & 3.5355 & 0.3125 & -0.2778 \\ -0.2549 & 0.6339 & -0.25 & 3.5355 & 0.3125 & -0.2778 \\ -0.2549 & -0.6339 & -0.25 & -3.5355 & 0.3125 & 0.2778 \\ -0.0987 & 1.1339 & 0.25 & 3.5355 & -0.3125 & 0.2778 \\ -0.0987 & -1.1339 & 0.25 & -3.5355 & -0.3125 & -0.2778 \end{bmatrix}\begin{bmatrix}\mathbf{F}_{desired}\\ \mathbf{T}_{desired}\end{bmatrix} \quad (2)$$

Since a thruster cannot develop negative thrust, the thrusters must all be biased to a positive value so that adding τ_{cmnd} results in an overall command between 2 μN and 20 μN for each thruster. Equation (2) clearly shows that the command authority is weakest for x-axis torque commands, which is already obvious from the thruster configuration shown in Figure 2. It is an important feature of the system design that the x-axis is parallel to the line between the proof masses, since this is the axis requiring the least dynamic torque authority, as no attitude adjustment in the x-direction is needed to follow the non-reference test mass.

Different disturbances are included in this model. The first is the nominal solar radiation pressure and its variation. The Sun exposed face of the spacecraft corresponds to the z direction. The angle of the incident rays of the sun to the surface normal may be arbitrarily assigned, but is assumed to be zero for the current analysis. The frequency spectrum used for solar radiation flux variations given in Figure 3 represents a conservative assessment of measured variations [4,5]. This plot indicates a constant spectrum at the frequencies below 0.1 mHz, followed by a $1/f$ roll off. This spectrum also includes the so-called 5-minute acoustic oscillation (at 3.5 mHz), and levels off at frequencies above 10 mHz.

The second disturbance source modeled was the acceleration noise on the test mass. A number of sources contribute to this acceleration noise, including magnetic and Lorentz forces, thermal disturbances, cosmic ray impacts, etc. The spectral density function for the test mass acceleration noise is assumed to have: $1/f^2$ roll-off at frequency range of 0.01-0.1 mHz, $1/f$ roll-off at frequency range of 0.1-1 mHz, and constant spectral density $3\text{x}10^{-14}$ m/s^2/$\sqrt{\text{Hz}}$ at frequencies above 1 mHz. The linear filter approximation to this frequency spectrum shown in Figure 4 meets or exceeds all disturbance levels. This acceleration noise was applied to both test masses in all directions in this analysis. White-noise models were used to capture thruster noise, electrostatic suspension force noise, star tracker noise, and the capacitive sensing noise (used to measure the positions of the test masses relative to the spacecraft). The intensity levels are captured in Table 1.

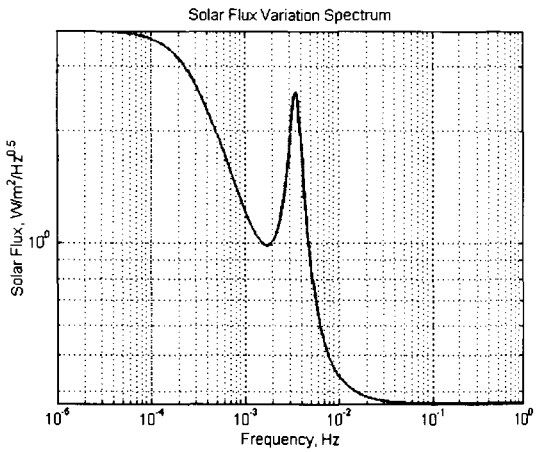

Figure 3 Root Power Spectrum of the Solar Radiation Flux Variation

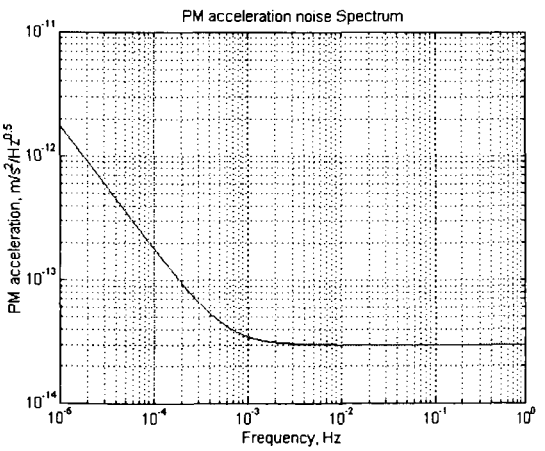

Figure 4 Root Power Spectrum for the Test Mass Acceleration Noise

Table 1 Actuation and Sensing Noise Intensities

Noise Source	Intensity
Thrusters	0.1 μN/Hz$^{0.5}$
Suspension Force	2×10^{-14} N/Hz$^{0.5}$
Star Tracker	20 arcsec/ Hz$^{0.5}$
Capacitive Sensing	3 nano-m/ Hz$^{0.5}$

CONTROLLER DESIGN

Currently, there are five modes envisioned for the spacecraft control in the ST7 Disturbance Reduction system. These are the Attitude Only mode, in which only the spacecraft attitude is controlled using star tracker (ST) data; Accelerometer mode, in which both spacecraft attitude and position are controlled using ST data as well as the acceleration signals from one of the gravitational sensors; First Drag-Free mode, which is the same as the previous mode except relative position errors from a GRS are used to establish drag-free motion of one test mass; Interim Drag-Free mode, which is the same as the First Drag-Free mode except acceleration signals from the second GRS unit are used to quiet the spacecraft about the second test mass; and finally the Science mode, in which both test masses are in drag-free motion in the measurement band. The science mode is the main control mode as well as the most complex. It is the mode presented and

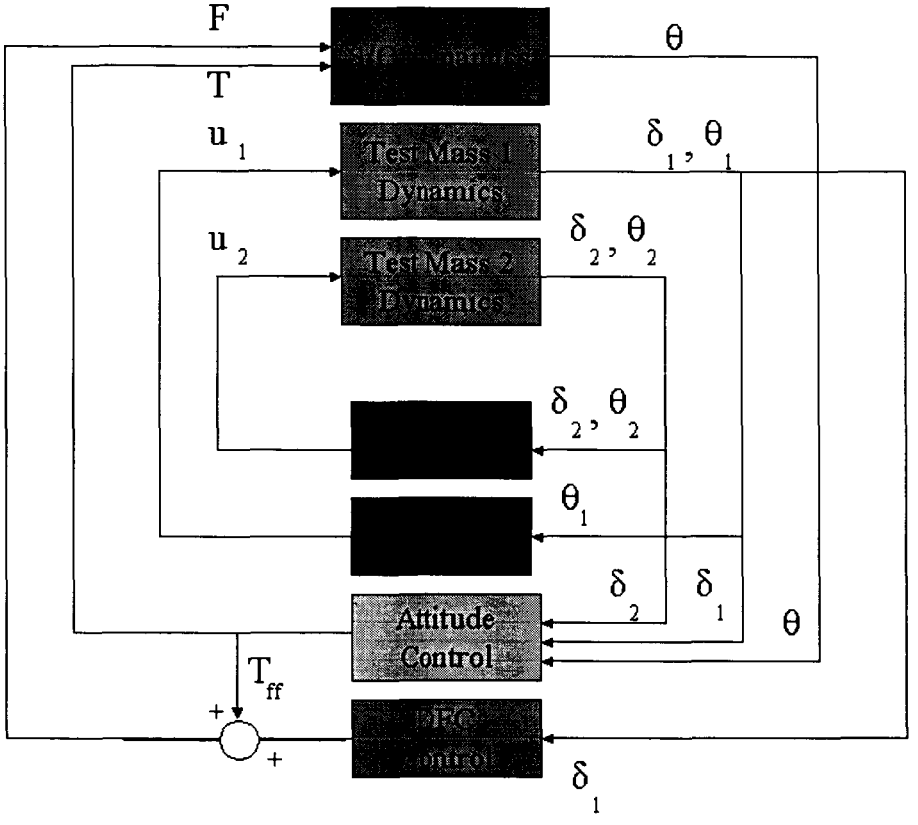

Figure 5 Block Diagram of the DRS Science Control Mode

discussed here. A top-level block diagram of the system dynamics is shown in Figure 5. The outputs of each GRS are the translational (δ) and rotational (θ) displacements of its test mass relative to the center of its housing. The inputs to each GRS are the suspension forces and torques, collected in a six-element vector u. The drag-free controller controls the position of the spacecraft to establish free-fall motion of one of the test masses. Either test mass can be chosen as the drag-free reference, but the analysis in this paper chooses test mass 1. The spacecraft attitude control orients the spacecraft in the low frequency band (DC and near DC) using the star tracker data, and centers the spacecraft about the other test mass (test mass 2 in this paper) in the transverse (y and z) directions in the measurement band. Both test masses are effectively freely falling in the ST7 science measurement band from 1 to 30 mHz. The 18-DOF Model also includes the electrostatic suspension control of the test masses. The controllers were designed using a classical single-input-single-output control approach, but the 18-DOF system is a multi-input-multi-output system by virtue of the cross coupling between the relative test mass positions and the attitude of the spacecraft.

The four control loops were implemented within a MATLAB-based model of the system. This MATLAB model serves as the design and analysis tool for the 18-DOF Model. The spacecraft control is referred to as the Dynamic Control System (DCS). The main performance requirements for the DCS in the science mode are summarized below:

- The DCS shall keep the spacecraft pointed to within 5° of a prescribed target (nominally the Sun).
- The DCS shall control the spacecraft position with respect to the drag-free reference test mass to better than 10 nm/√Hz over the frequency range of 1 mHz to 30 mHz.
- The DCS shall control the spacecraft attitude to maintain the position of the non-reference test mass with respect to its housing to better than 10 nm/√Hz over the frequency range of 1 mHz to 30 mHz, in the transverse directions.
- The drag-free control shall limit spacecraft acceleration to keep force levels on both test masses within the GRS electrostatic suspension limits.
- The drag-free control commands to the individual thrusters shall be within 2 to 20 μN.

All sensor measurements are updated at 10 Hz sampling with the exception of the star tracker signal, which is updated at 1 Hz sampling. There are four control loops, controlling the attitude and position of the spacecraft as well as the relative attitude and position of the two test masses. The attitude control loop is a 7-input/3-output controller, which uses the three attitude errors (obtained from ST measurement) and the relative position errors of the test masses in the transverse directions to compute the required spacecraft torque commands.

$$T(s) = K_{al}(s)\theta(s) + K_{ah}(s)\begin{Bmatrix} y_1(s) \\ z_1(s) \\ y_2(s) \\ z_2(s) \end{Bmatrix} \tag{3}$$

Here, controller $K_{al}(s)$ denotes the low-bandwidth part of the attitude control designed to maintain the attitude of the spacecraft. It is a PID controller with an appropriate attenuation filter, resulting in a 5th-order controller (crossover frequency @ 0.00001 Hz). Controller $K_{ah}(s)$ represents the part of the attitude controller responsible for centering the spacecraft about the non-reference test mass in the transverse directions. The relative position error of the test masses in the transverse direction are used to compute the required rotation (in GRS frame) of the GRS package about the drag-free reference test mass. The required rotation command is then transformed into S/C frame and is used as an input to a SISO-based controller to regulate the S/C attitude in the science band. To obtain a pure rotation about the first test mass, feedforward translation commands are generated and issued to the drag-free controller. Controller $K_{ah}(s)$ is also designed based on the classical approach, and is a series combination of lead-lag filter, PD filter, and a roll-off filter, resulting in a 7th-order controller.

The second control loop is the drag-free controller. This controller was designed using classical control approach, resulting in crossover frequencies between 0.055 and 0.06 Hz. Feedforward compensation is implemented in the drag-free loop (a) to allow for pure rotation of the GRS about one test mass, and (b) to reduce the attitude/translation couplings. The controller is given by

$$u_{DFC}(s) = K_{DFC}(s)y_1(s) + \vec{p}_1 \times [H * T(s)] \tag{4}$$

Where $K_{DFC}(s)$ denotes the drag-free controller, the vector $\mathbf{p}_1$ represents the position of test mass 1 relative to the system center of mass, and H is a matrix which depends on spacecraft inertia and mass properties.

The suspension control system, which maintains the relative attitude of both test masses (with respect to their respective housings) and the relative position of the non-reference test mass, is an integral part of the GRS, so it is not part of the control software reported in this paper. However, it is necessary to develop the

suspension control and drag-free controls together and to demonstrate their compatibility. Preliminary control designs and noise models provided by the GRS developers were modified for this analysis to accommodate stability margin requirements of the coupled ST7/DRS control system. The compatibility of the final GRS suspension control and the drag-free control will be validated in a closed-loop simulation. The suspension controllers were low bandwidth controllers which were designed using classical methods to provide disturbance rejection for the 2nd test mass at DC and near DC, while ensuring that no significant residual acceleration are present in the ST7-DRS science band. The suspension controllers were also designed to handle the electrostatic stiffness effects.

Stability Margins

The block diagram of the system in Figure 5 shows 15 outputs and 15 inputs. The 15 measurements used by the control system are the spacecraft attitude error from the star tracker, relative position and attitude of the drag-free reference test mass, and the relative position and attitude of the other test mass. The 15 control inputs are the thruster force and torque commands in the spacecraft frame, the suspension control torque commands for the drag-free reference test mass, and the suspension control force and torque commands for the other test mass. The controller for each loop was designed independently using classical design techniques. However, the 18-DOF model, by the virtue of cross coupling between relative test mass positions and the attitude of the spacecraft, represents a multi-input-multi-output system. Hence, the loop gains for each input and output channel (while the remaining channels are closed) must be analyzed for proper stability margins. Each control loop was required to have a phase margin of at least 35° and a gain margin of at least 6 dB in magnitude. The margins are shown in Table 2, and they satisfy these requirements. Note that the requirements are still satisfied with the negative gain margin for the thrust torque command in y-direction.

Table 2 Gain and Phase Margins

Channel	Gain Margin (dB)	Phase Margin (deg)
Star tracker output - *x*	18	55
Star tracker output - *y*	10	39
Star tracker output - *z*	10	37
Test mass 1 position relative to housing - *x*	6	36
Test mass 1 position relative to housing - *y*	6	35
Test mass 1 position relative to housing - *z*	6	35
Test mass 2 position relative to housing - *x*	27	48
Test mass 2 position relative to housing - *y*	9	39
Test mass 2 position relative to housing - *z*	9	37
Test mass 1 attitude relative to housing - *x*	22	51
Test mass 1 attitude relative to housing - *y*	22	51
Test mass 1 attitude relative to housing - *z*	22	51
Test mass 2 attitude relative to housing - *x*	22	51
Test mass 2 attitude relative to housing - *y*	22	51
Test mass 2 attitude relative to housing - *z*	22	51
Thrust torque command - *x*	18	54
Thrust torque command - *y*	–8	37
Thrust torque command - *z*	9	39
Thrust force command - *x*	6	36
Thrust force command - *y*	6	35
Thrust force command - *z*	6	35
Test mass 2 suspension force command - *x*	27	48
Test mass 2 suspension force command - *y*	9	58
Test mass 2 suspension force command - *z*	8	53

Test mass 1 suspension torque command - x	22	51
Test mass 1 suspension torque command - y	22	51
Test mass 1 suspension torque command - z	22	51
Test mass 2 suspension torque command - x	22	51
Test mass 2 suspension torque command - y	22	51
Test mass 2 suspension torque command - z	22	51

ANALYSIS RESULTS AND DISCUSSION

Both time-domain and frequency-domain analyses were performed. The root power spectral density (PSD) plots in Figures 6-23 show the contributions of the various disturbance sources. The contribution of each disturbance category represents the root sum squared (RSS) values for that category; for example, the thruster noise plot is the RSS contribution of the noise from all eight thrusters. Figures 6-11 illustrate the root PSDs of the relative positions of both test masses with respect to their respective housings. These relative positions must obey a PSD requirement of 10 nm/$\sqrt{\text{Hz}}$ for both test masses in the science band, which is the most stringent requirement on the ST7 drag-free control. This required performance level is along the top of the plot in Figures 6-8, and is indicated by a horizontal dashed line in Figures 9-11. The plots show that the system satisfies these stringent requirements, with spectra being mainly dominated by the thruster noise and measurement noise. It is possible to reduce the peak PSDs in the vicinity of 30 mHz at the expense of requiring more high-frequency thruster activity; the current design is a near-optimal compromise of these requirements. The root PSD of the relative position of test mass 1 is also below 10 nm/$\sqrt{\text{Hz}}$ at all frequencies below the measurement band, but the root PSD of the relative position of test mass 2 exceeds this level at DC and near DC frequencies. This is unavoidable along the GRS axis with the ST7 GRS orientations, since it is impossible for both proof masses to be drag-free simultaneously at low frequencies while remaining centered in their housings. It is also unavoidable in the transverse directions because the spacecraft attitude control is tasked to properly point the spacecraft at DC and near DC frequencies, and the suspension control system's bandwidth is restricted to avoid actuation cross-talk inducing accelerations in the sensitive axis.

Figures 12-17 illustrate the spectra for the spacecraft thruster force and torque commands. The RSS levels are mainly dominated by the thruster noise in the measurement band and at lower frequencies. Capacitive sensing noise makes the largest contribution to the variations in the thrust force and y and z axis thrust torque commands above the measurement band, especially in the 100-200 mHz range. The x axis thrust torque command falls off much more rapidly than the other thrust commands in and above the measurement band, reflecting the much looser requirements on x axis rotations. As mentioned above, the thruster layout was configured with these looser x-axis requirements in mind. The root PSDs for individual thruster commands were computed but are not presented in this paper. They are very similar in both magnitude and frequency dependence to the thruster force commands shown in Figures 12-14, indicating significant thruster activity in the 100-200 mHz frequency range.

The root PSDs of the spacecraft attitude pointing errors are shown in Figures 18-20. Although, the requirement on the spacecraft pointing is fairly coarse, these figures indicate a fairly tight steady-state pointing performance. They are almost completely dominated by thruster noise.

The root PSDs of the suspension forces for test mass 2, illustrated in Figures 21-23, are within acceptable range of accelerations on the test masses ($3\text{x}10^{-14}$ (1 + [f/3 mHz]^2) m/s^2/$\sqrt{\text{Hz}}$). They are dominated by thruster noise up to 0.1 Hz and by capacitive sensing noise above that frequency. The root PSDs of the suspension forces for test mass 1 are identically zero in this analysis, since no suspension forces are applied to the drag-free test mass. The PSDs of the test mass relative attitude errors and suspension torques were computed but are not presented in this paper. Again, the suspension controllers used in the analysis are placeholders. The actual controllers are being designed by the GRS team.

Time-domain analyses of the control systems were also performed with the 18-DOF Model. The gap response histories and the spacecraft attitude histories are not presented here because; (a) they take a long time to reach steady state (due to very small loop bandwidths), and (b) it is hard to discern from time histories that frequency-dependent performance measures are met. The time histories of the command variations for the eight thrusters are presented in Figures 24-31. The thruster command variations are about a slow varying set point that takes up to 100 seconds to move from 2 μN to 20 μN, or the reverse. Fast thruster command changes (10 Hz rate) are limited to ±20% of the set point value, hence one needs to know the worst-case peak-to-peak command variations in the time scale of set point changes in order to choose the set point values properly. A short (100 second) segment of the time history of the commands for thruster no. 3 is provided in Figure 32 to show its temporal behavior more clearly. As expected, the thruster commands are dominated by frequencies in 100-200 mHz range.

CONCLUDING REMARKS

Preliminary designs for the spacecraft attitude, and drag-free control systems have been completed. An 18-DOF model of the ST7 Disturbance Reduction System, which includes full rigid-body dynamics of the spacecraft and two test masses, has been developed and was used to perform control design and validation. Both time-domain and frequency-domain analyses indicate that the ST7 DRS requirements can be met. These include establishing drag-free motion of the test masses in the science band as well as spacecraft attitude control. The spacecraft position relative to the primary test mass can be maintained within the required precise limits. These analyses have also shown that it is possible to electrostatically suspend the second test mass while maintaining its drag-free state within the frequency range of interest, by rapidly rolling off suspension forces between DC and the measurement frequency band. Successful spacecraft attitude control is accomplished by combining low frequency data from a star tracker and high frequency data from the transverse position of the second test mass.

REFERENCES

[1] Keiser, G. M., Buchman, S., Byer, R. L., Folkner, W. M., Hruby, V., and Gamero-Castaño, M., "Disturbance Reduction System for Testing Technology for Drag-Free Operation," SPIE Paper 4856-02, Astronomical Telescopes and Instrumentation Conference, Waikoloa, Hawaii, USA, August 2002.

[2] Maghami, P. G., Markley, F. L., Dennehy, C. J., Houghton, M. B., and Folkner, W. M., "Controller Design for the ST7 Disturbance Reduction System," 5th International Conference on Guidance, Navigation, and Control Systems, Frascati, Italy, Oct. 22–25, 2002

[3] Maghami, P. G., Markley, F. L., Houghton, M. B., and Dennehy, C. J., "Design and Analysis of the ST7 Disturbance Reduction System (DRS) Spacecraft Controller," AAS 03-165, AAS Guidance and Control Conference, Breckenridge, CO, Feb. 5–9, 2003

[4] J. Pap, et. al., "Variation in Total Solar and Spectral Irradiance as Measured by the VIRGO Experiment on SOHO", *Adv. Space Res.*, 24:215-224, 1999.

[5] LISA: Laser Interferometer Space Antenna, System and Technology Status Report, ESA-SCI(2000)11, July 2000.

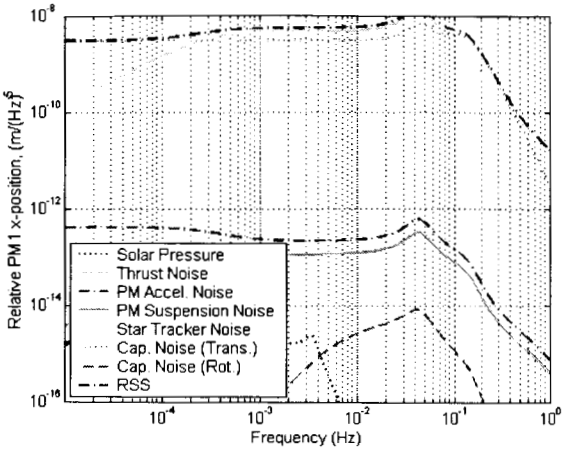

Figure 6 Root Power Spectrum of the Relative Position of Test Mass 1: *x*-Direction

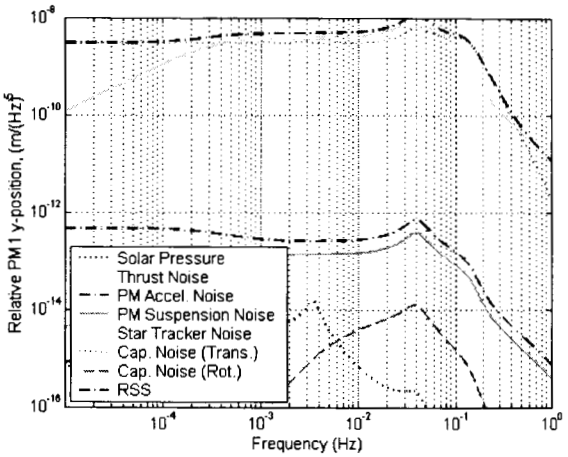

Figure 7 Root Power Spectrum of the Relative Position of Test Mass 1: *y*-Direction

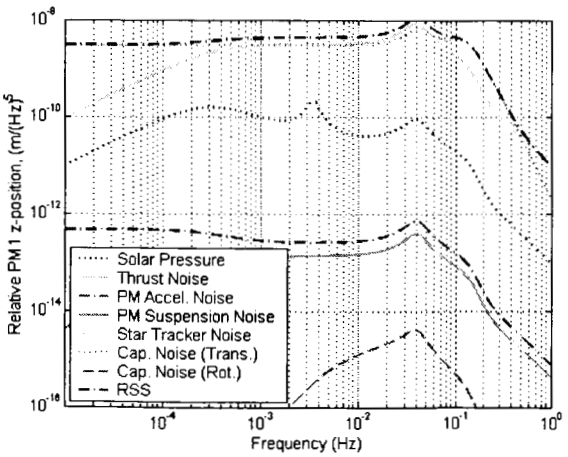

Figure 8 Root Power Spectrum of the Relative Position of Test Mass 1: *z*-Direction

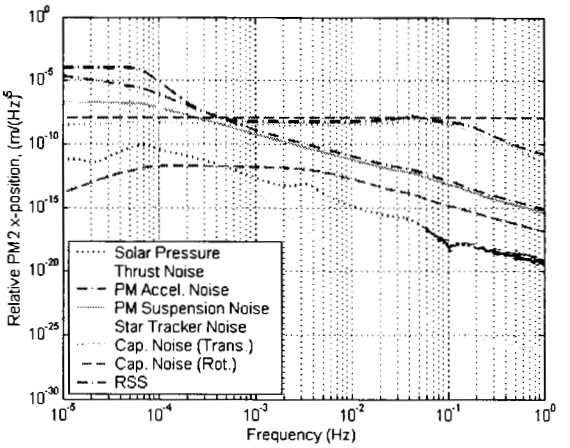

Figure 9 Root Power Spectrum of the Relative Position of Test Mass 2: *x*-Direction

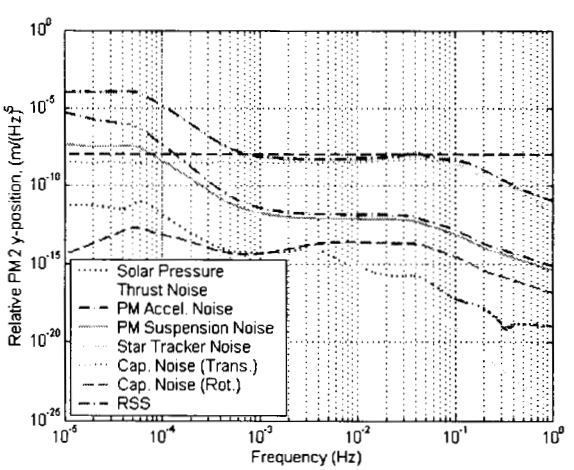

Figure 10 Root Power Spectrum of the Relative Position of Test Mass 2: *y*-Direction

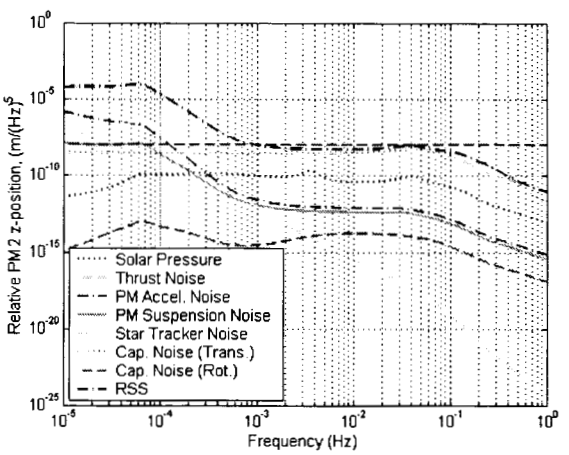

Figure 11 Root Power Spectrum of the Relative Position of Test Mass 2: *z*-Direction

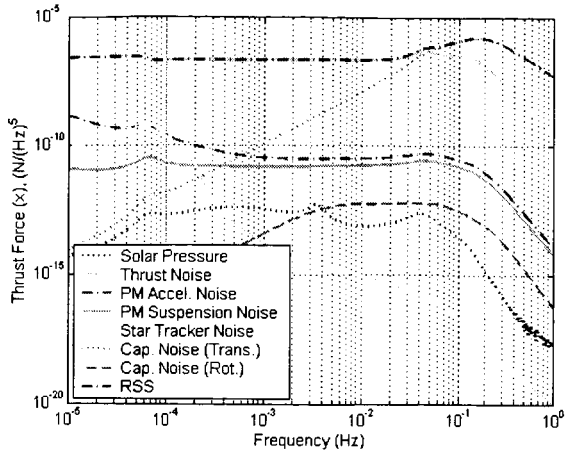

Figure 12 Root Power Spectrum of the Thrust Force: *x*-Direction

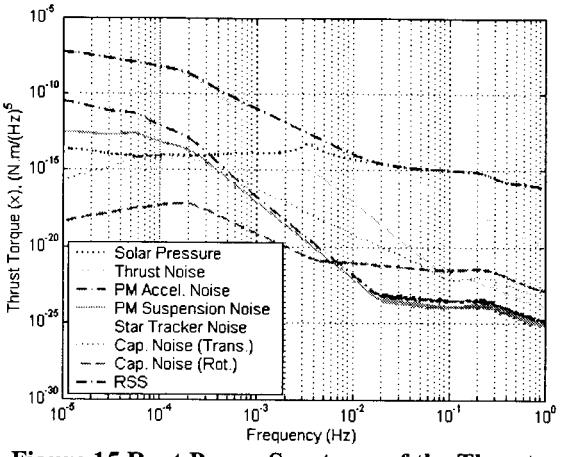

Figure 15 Root Power Spectrum of the Thrust Torque: *x*-Direction

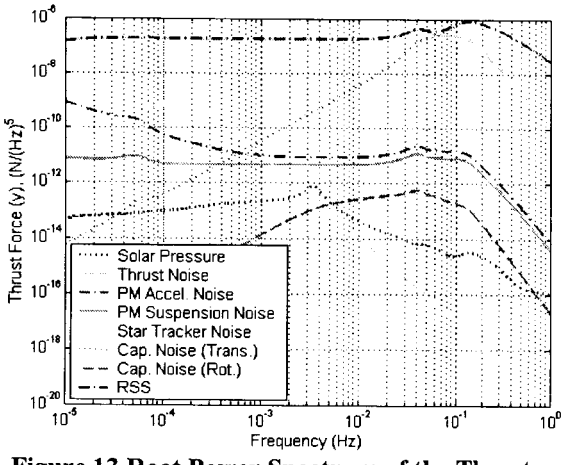

Figure 13 Root Power Spectrum of the Thrust Force: *y*-Direction

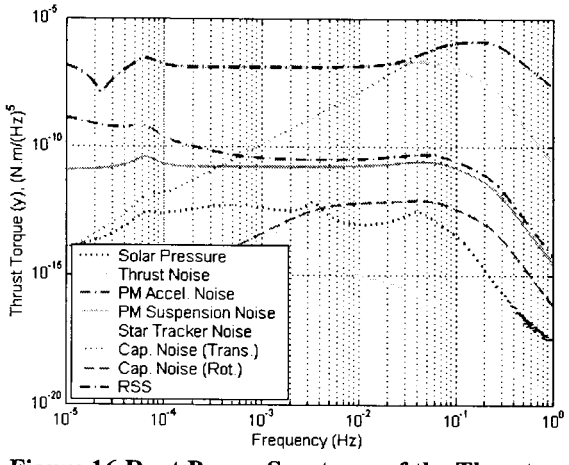

Figure 16 Root Power Spectrum of the Thrust Torque: *y*-Direction

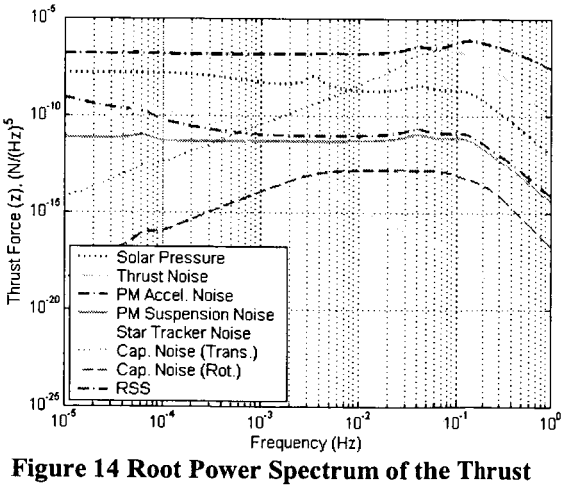

Figure 14 Root Power Spectrum of the Thrust Force: *z*-Direction

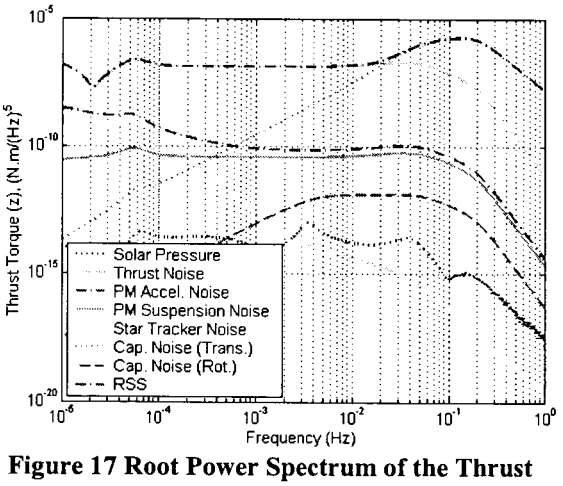

Figure 17 Root Power Spectrum of the Thrust Torque: *z*-Direction

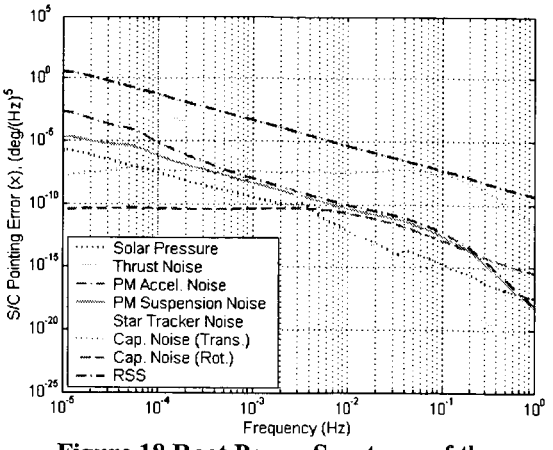

Figure 18 Root Power Spectrum of the Spacecraft Attitude Error: *x*-Direction

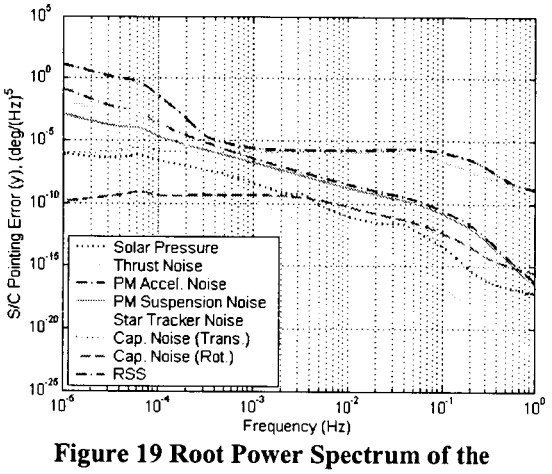

Figure 19 Root Power Spectrum of the Spacecraft Attitude Error: *y*-Direction

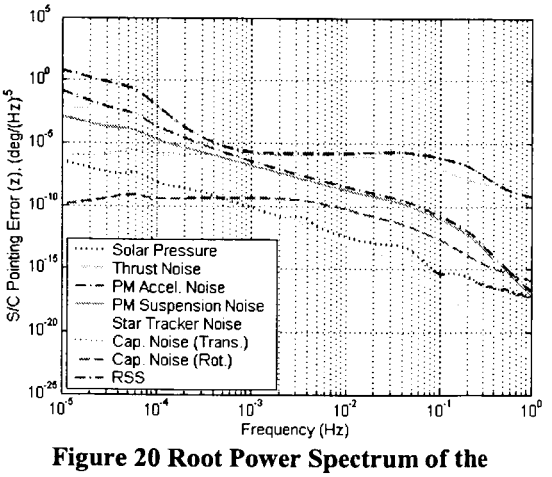

Figure 20 Root Power Spectrum of the Spacecraft Attitude Error: *z*-Direction

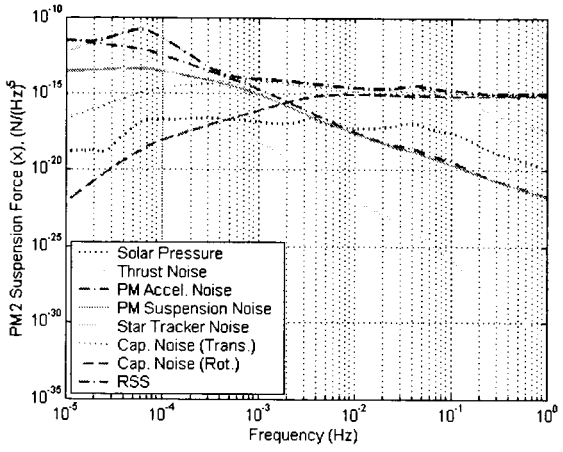

Figure 21 Root Power Spectrum of the Test Mass 2 Suspension Force - *x*

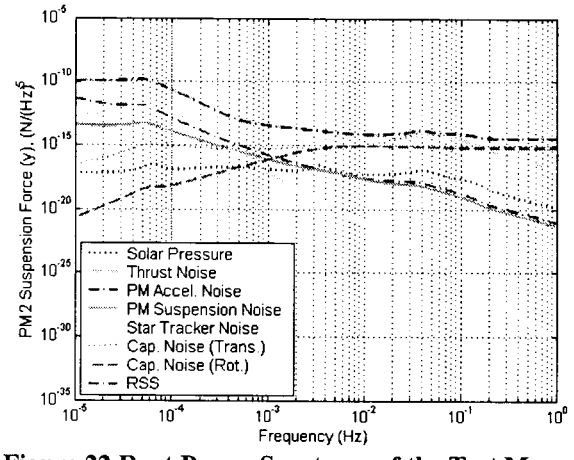

Figure 22 Root Power Spectrum of the Test Mass 2 Suspension Force - *y*

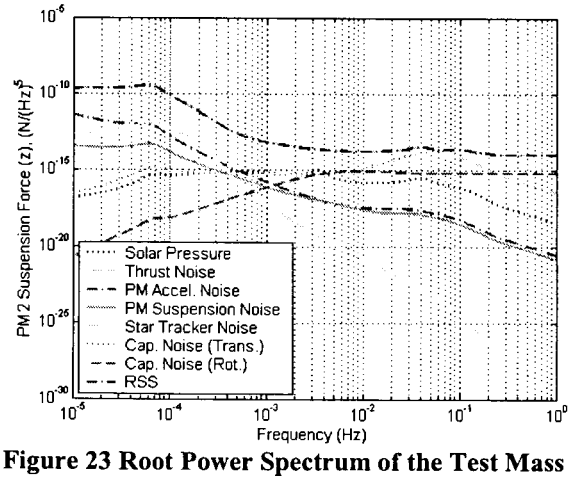

Figure 23 Root Power Spectrum of the Test Mass 2 Suspension Force - z

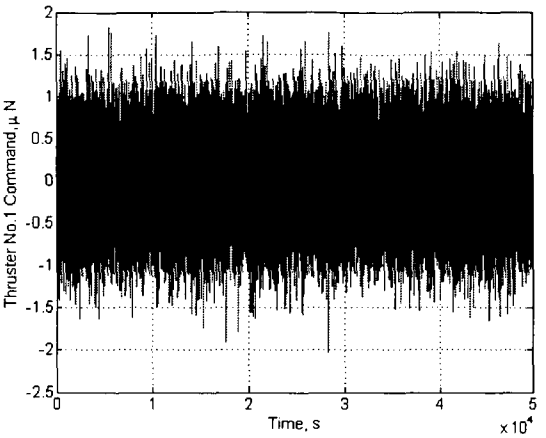

Figure 24 Time History of Thruster No. 1 Command Variations

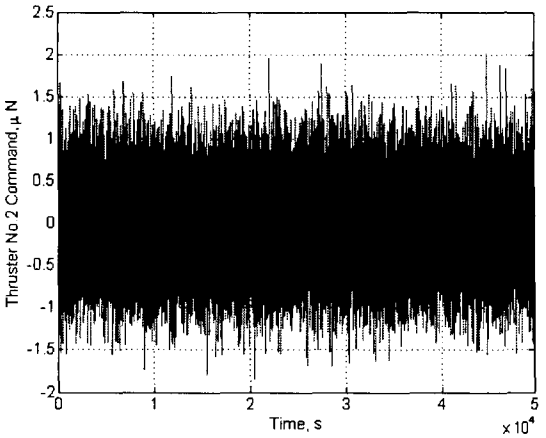

Figure 25 Time History of Thruster No. 2 Command Variations

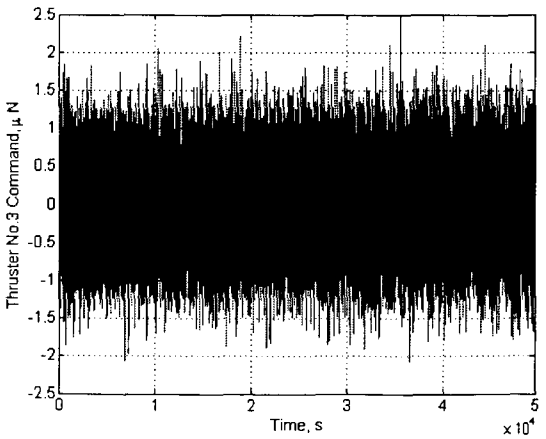

Figure 26 Time History of Thruster No. 3 Command Variations

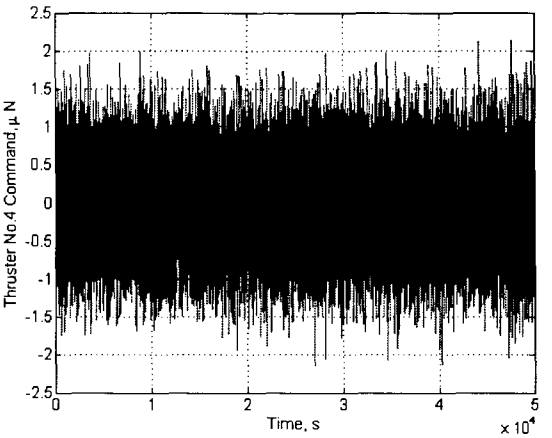

Figure 27 Time History of Thruster No. 4 Command Variations

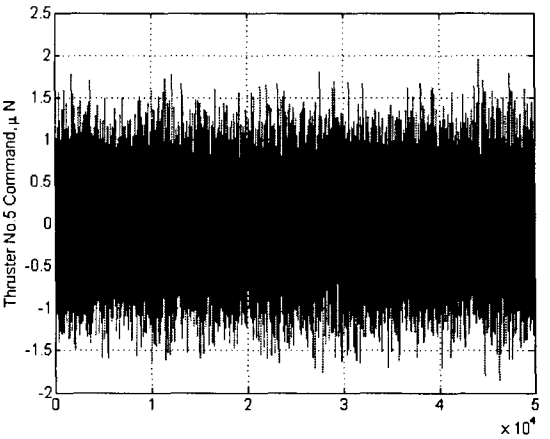

Figure 28 Time History for Thruster No. 5 Command Variations

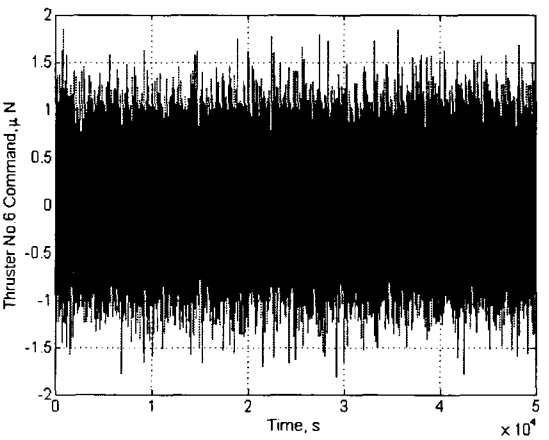

Figure 29 Time History of Thruster No. 6 Command Variations

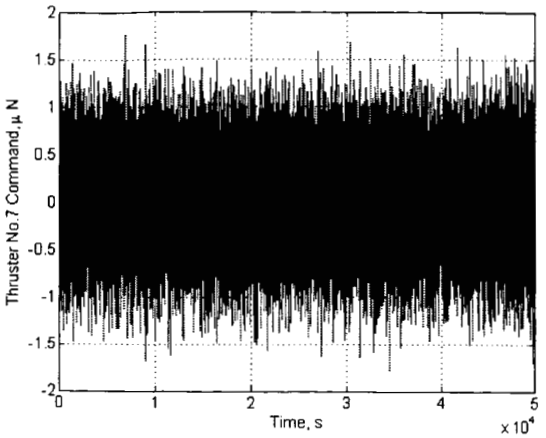

Figure 30 Time History of Thruster No. 7 Command Variations

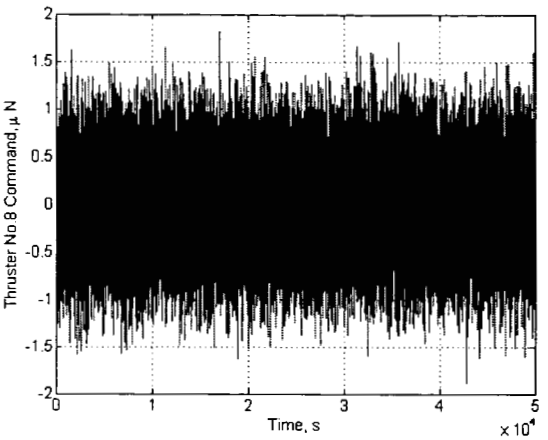

Figure 31 Time History of Thruster No. 8 Command Variations

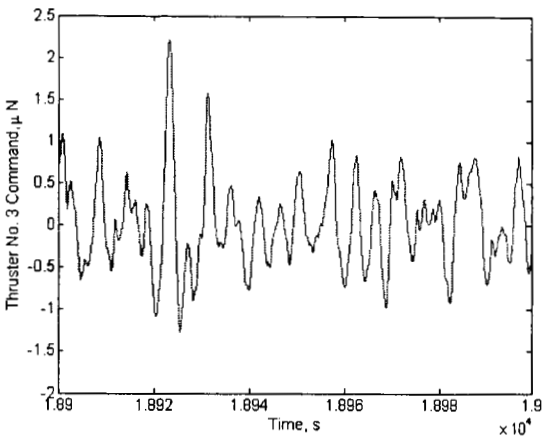

Figure 32 Time History of Thruster No. 3 Command Variations